

DTIC FILE COPY

4

David Taylor Research Center

Bethesda, MD 20084-5007

AD-A198 781

DTRC-88/031 August 1988

Ship Hydromechanics Department
Research and Development Report

A Potential Flow Solution on Marine Propeller and Axial Rotating Fan

by

Y.T. Lee

C.W. Jiang

T.W. Bein

DTRC-88/031 A Potential Flow Solution on Marine Propeller and Axial Rotating Fan

DTIC
ELECTE
SEP 23 1988
S H D



Approved for public release; distribution is unlimited.

88 9 23 052

MAJOR DTRC TECHNICAL COMPONENTS

- CODE 011 DIRECTOR OF TECHNOLOGY, PLANS AND ASSESSMENT
 - 12 SHIP SYSTEMS INTEGRATION DEPARTMENT
 - 14 SHIP ELECTROMAGNETIC SIGNATURES DEPARTMENT
 - 15 SHIP HYDROMECHANICS DEPARTMENT
 - 16 AVIATION DEPARTMENT
 - 17 SHIP STRUCTURES AND PROTECTION DEPARTMENT
 - 18 COMPUTATION, MATHEMATICS & LOGISTICS DEPARTMENT
 - 19 SHIP ACOUSTICS DEPARTMENT
 - 27 PROPULSION AND AUXILIARY SYSTEMS DEPARTMENT
 - 28 SHIP MATERIALS ENGINEERING DEPARTMENT

DTRC ISSUES THREE TYPES OF REPORTS:

1. **DTRC reports, a formal series**, contain information of permanent technical value. They carry a consecutive numerical identification regardless of their classification or the originating department.
2. **Departmental reports, a semiformal series**, contain information of a preliminary, temporary, or proprietary nature or of limited interest or significance. They carry a departmental alphanumerical identification.
3. **Technical memoranda, an informal series**, contain technical documentation of limited use and interest. They are primarily working papers intended for internal use. They carry an identifying number which indicates their type and the numerical code of the originating department. Any distribution outside DTRC must be approved by the head of the originating department on a case-by-case basis.

UNCLASSIFIED

SECURITY CLASSIFICATION OF THIS PAGE

REPORT DOCUMENTATION PAGE				
1a. REPORT SECURITY CLASSIFICATION UNCLASSIFIED		1b. RESTRICTIVE MARKINGS		
2a. SECURITY CLASSIFICATION AUTHORITY		3. DISTRIBUTION/AVAILABILITY OF REPORT Approved for public release; distribution is unlimited.		
2b. DECLASSIFICATION/DOWNGRADING SCHEDULE				
4. PERFORMING ORGANIZATION REPORT NUMBER(S) DTRC-88/031		5. MONITORING ORGANIZATION REPORT NUMBER(S)		
6a. NAME OF PERFORMING ORGANIZATION David Taylor Research Center	6b. OFFICE SYMBOL (if applicable) Code 1542	7a. NAME OF MONITORING ORGANIZATION		
6c. ADDRESS (City, State, and ZIP Code) Bethesda, MD 20084-5000		7b. ADDRESS (City, State, and ZIP Code)		
8a. NAME OF FUNDING/SPONSORING ORGANIZATION	8b. OFFICE SYMBOL (if applicable)	9. PROCUREMENT INSTRUMENT IDENTIFICATION NUMBER		
8c. ADDRESS (City, State, and ZIP Code)		10. SOURCE OF FUNDING NUMBERS		
		PROGRAM ELEMENT NO	PROJECT NO	TASK NO
				WORK UNIT ACCESSION NO
11. TITLE (Include Security Classification) A Potential Flow Solution on Marine Propeller and Axial Rotating Fan				
12. PERSONAL AUTHOR(S) Lee, Y.T., Jiang, C.W., and Bein, T.W.				
13a. TYPE OF REPORT Final	13b. TIME COVERED FROM _____ TO _____	14. DATE OF REPORT (Year, Month, Day) 1988 August	15. PAGE COUNT 32	
16. SUPPLEMENTARY NOTATION				
17. COSATI CODES			18. SUBJECT TERMS (Continue on reverse if necessary and identify by block number) Pump, Integral Equation, Propeller, Lifting Surface, Potential Flow, Vortex. <i>DES</i>	
FIELD	GROUP	SUB-GROUP		
19. ABSTRACT (Continue on reverse if necessary and identify by block number) Integral equations are derived to model the solid surfaces and the inlet condition for both external and internal flows with an axially rotating element. Vortex filaments are used to simulate the lifting surfaces. Global iterations for surface-panel source densities and vortex strengths are used in conjunction with the Neumann iterations for solving integral equations. A special kernel treatment is adopted in the solution scheme of the integral equation. Solutions converge within 10-20 iterations. Calculated results and measured data for a propeller tested in open water are in good agreement. Predictions are also made for an axial-flow pump. The overall performance parameters for the pump agree within a few percent of the design values. <i>Keywords</i>				
20. DISTRIBUTION/AVAILABILITY OF ABSTRACT <input checked="" type="checkbox"/> UNCLASSIFIED/UNLIMITED <input type="checkbox"/> SAME AS RPT <input type="checkbox"/> DTIC USERS		21. ABSTRACT SECURITY CLASSIFICATION UNCLASSIFIED		
22a. NAME OF RESPONSIBLE INDIVIDUAL Yu-Tai Lee		22b. TELEPHONE (Include Area Code) (301) 227-1340	22c. OFFICE SYMBOL Code 1542	

CONTENTS

	Page
SYMBOLS.....	iv
ABSTRACT.....	1
ADMINISTRATIVE INFORMATION.....	1
INTRODUCTION.....	1
MATHEMATICAL MODEL.....	3
STATEMENT OF PROBLEM.....	3
METHOD OF APPROACH.....	4
INTEGRAL EQUATION FOR SOURCE-STRENGTH DETERMINATION.....	5
VORTEX FIELD AND ITS DISTRIBUTION.....	7
NUMERICAL ITERATION.....	11
NUMERICAL EXAMPLES.....	11
GEOMETRY INPUTS.....	12
NUMERICAL RESULTS.....	13
CONCLUSIONS.....	19
REFERENCES.....	21

FIGURES

1. Definition sketch.....	3
2. Vortex distribution on a lifting surface.....	4
3. Definition sketch for a vortex filament.....	7
4. Calculated pressure distributions for NACA 0012 foil at $\alpha = 10^\circ$	8
5. Calculated pressure distributions for NACA 66-209 foil at $\alpha = 2^\circ$	9
6. Paneling on the marine propeller.....	12
7. Paneling on the axial-flow pump.....	13

FIGURES (Continued)

	Page
8. Wake vortex filaments and grids of one sector for Propeller 4718 at $J = 0.751$	13
9. Pressure distributions on Propeller 4718 at $J = 0.751$	15
10. Pressure distributions on Propeller 4718 at different values of J	16
11. Wake vortex filaments and grids of one sector for axial-flow pump at $c = 0.292$	17
12. Calculated blade pressure distributions for axial-flow pump at $c = 0.292$	18
13. Computed transverse-velocity distribution	19

SYMBOLS

c	flow coefficient, defined as the ratio of V_{∞} to the blade tip speed
C_p	pressure coefficient
D	blade diameter
f	$V_N - V_{TN}$
g	function defined by Equation (13)
\bar{h}	vortex segment
J	advance coefficient
K	kernel or Kutta point
M	strength of source
n	number of global iteration
N	surface normal
$\bar{r} (r)$	position vector or radius
s	spanwise distance
S	surfaces
t	blade trailing edge

SYMBOLS (Continued)

T blade thickness
 \bar{V} velocity vector
 Ψ domain of calculation
 x, y, z global coordinates
 α $\int_S K(Q, P) dS_Q$
 γ bound vortex strength along spanwise direction
 Γ strength of vortex filament
 θ azimuthal angle
 κ surface curvature
 \bar{E} position vector
 ϕ velocity potential
 $\bar{\omega}$ rotational velocity



Accession For	
NTIS GRA&I	<input checked="" type="checkbox"/>
DTIC TAB	<input type="checkbox"/>
Unannounced	<input type="checkbox"/>
Justification	
By _____	
Distribution/ _____	
Availability Codes	
Dist	Avail and/or Special
A-1	

ABSTRACT

Integral equations are derived to model the solid surfaces and the inlet condition for both external and internal flows with an axially rotating element. Vortex filaments are used to simulate the lifting surfaces. Global iterations for surface-panel source densities and vortex strengths are used in conjunction with the Neumann iterations for solving integral equations. A special kernel treatment is adopted in the solution scheme of the integral equation. Solutions converge within 10-20 iterations. Calculated results and measured data for a propeller tested in open water are in good agreement. Predictions are also made for an axial-flow pump. The overall performance parameters for the pump agree within a few percent of the design values.

ADMINISTRATIVE INFORMATION

This research was funded by the Surface Ship and Submarine Technology Program, PE62121N Block NDIA and PE62323N Block ND3A, respectively, administered by the David Taylor Research Center, Code 0124.

INTRODUCTION

It has become a requirement in the design process to obtain numerical solutions for an external or an internal flow past a rotating element with lift-generating surfaces; e.g., marine or aircraft propellers, turbine or pump impellers. Although a complete viscous solution technique would be a most desirable tool to achieve design accuracy, a number of difficulties exist in its applications. These difficulties include computer time and memory requirements, numerical solution procedures, turbulence modeling and lack of experience in handling such complex computer codes. Because of its modest complexity and reasonable computational time, an inviscid solution is therefore often pursued in the direct design process. In many cases, the accuracy of the inviscid solution is adequate for design. For the inviscid-flow model, Miranda [1] has compared the pros and cons between the potential

and the Euler solution procedures. In general, the selection of a numerical solution procedure is often case dependent, and no conclusive argument can easily be made. Significant reductions of the efforts in grid generation, engineering and computer time, and computer memory requirements promote the adoption of the potential solution using a surface-panel singularity method [2] instead of solutions using either a finite difference or a finite-element procedure [3].

The vortex-lattice method [4] has been used to model the axial flow through a marine propeller for many years. Realizing the shortcoming of this approach in representing arbitrary, thick surfaces, reference [4] was extended [5,6] to include the influence of the dominant thickness-effect components; e.g. hub and duct for the propeller. In recent years, Hess [7] has successfully applied his earlier development [8] to aircraft and marine propellers, using a source density on all on-body panels and a dipole density on lifting-surface panels. Maskew [9] extended Morino's [10] approach, which uses Green's Identity to determine a unique source-doublet specification, to the helicopter rotor problem. Nathman [11] also applies Morino's approach to the internal-flow problem. The drawback for Nathman's application is that Green's Identity is only valid for a closed domain. This restriction imposes a requirement of boundary conditions at the downstream outlet section for the internal-flow calculation. In general, the outlet conditions are part of the solution, and it is difficult to predetermine them.

In this report, integral equations for surface-source densities are derived and compared for both external and internal flows with an axially rotating element. For internal flows, integral equations are formulated for nonuniform inlet flow and "free" (i.e., no prerequisite conditions) outlet flow. Various strength distributions for the vortex filaments are examined and compared to achieve an optimal representation of the lifting surfaces. A numerical formula using the Biot-Savart law

for the evaluation of the velocity field due to a vortex segment is derived. Global iteration between the source and the vortex strengths is used in conjunction with the iterative scheme for solving the integral equation. A special treatment [12] to eliminate the singularity of the kernel of the integral equation is adopted. Two numerical examples, one for a marine propeller and one for an axial-flow pump, are presented.

MATHEMATICAL MODEL

STATEMENT OF PROBLEM

The problem being considered is the determination of the incompressible axial flow field through a rotating element with lifting surfaces. The flow can be either unbounded or bounded by a duct. The domain of interest Ψ , see Fig. 1, may or may

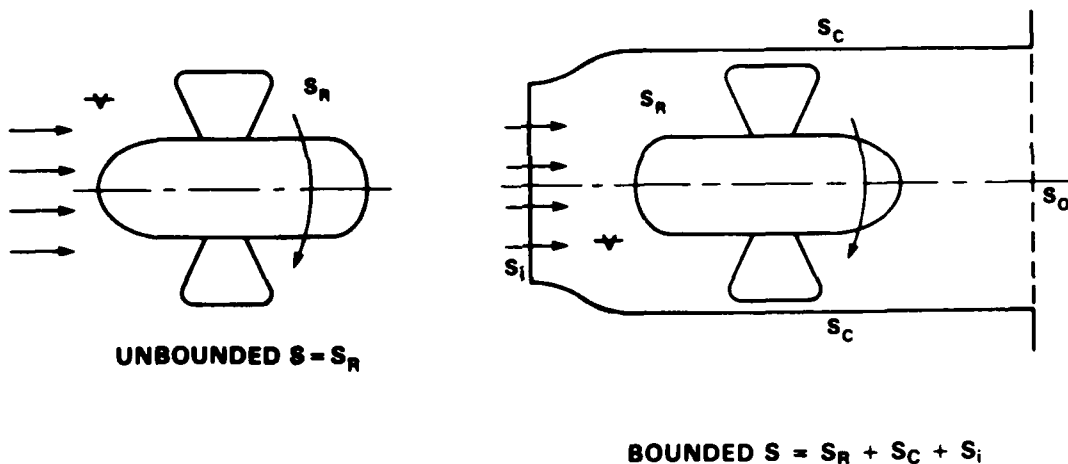


Fig. 1. Definition sketch.

not be simply connected. The boundary surfaces, S , may consist of rotating or nonrotating inner surfaces S_R and/or outer boundary surfaces S_I and S_C : $S = S_R + S_C + S_I$. The boundary conditions at the outer surface S_C and the nonrotating inner surfaces S_R are flow impermeable conditions, i.e.,

$$V_N = 0 \quad (1a)$$

where N is in the surface normal direction and directed into Ψ . For the rotating inner surface, the fluid velocity in the N -direction is

$$V_N = (\bar{\omega} \times \bar{r})_N \quad (1b)$$

where $\bar{\omega}$ is the rotational velocity and \bar{r} is the positional vector. The outer boundary surface S_1 is a permeable surface used to describe the nonuniformity of the inlet condition for internal flow,

$$V_N = V_{in} . \quad (1c)$$

METHOD OF APPROACH

The method of singularities is utilized for the solution of this rotating-flow field problem. To satisfy the boundary conditions (1), sources/sinks are distributed on all the inner surfaces and also on the outer surfaces for a bounded flow case. To satisfy the wake tangency condition at the sharp trailing edge of the lifting-surface element, as shown in Fig. 2, vortex filaments are distributed along the mean lines of the cross sections of the lifting surfaces as well as in the wake.

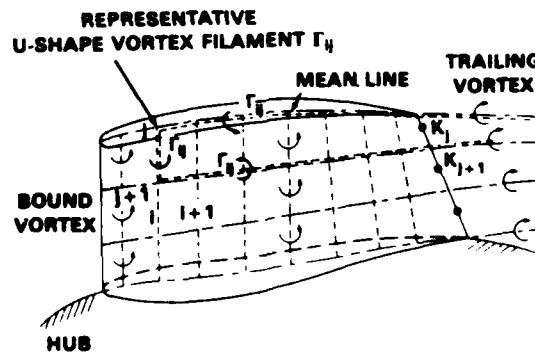


Fig. 2. Vortex distribution on a lifting surface.

Denote the velocity vector due to the surface-distributed sources by \bar{V}_M and that due to all the vortex filaments by \bar{V}_Γ . We then have

$$\bar{V} = \nabla\phi = \bar{V}_M + \bar{V}_\Gamma, \quad (2)$$

and

$$\bar{V}_M = \nabla \int_S -\frac{M(Q)}{r_{PQ}} dS_Q, \quad (3)$$

$$\bar{V}_\Gamma = \sum_i \sum_j \int_L \frac{\Gamma_{ij}(Q)}{4\pi} \frac{d\bar{a}_Q \times \bar{r}_{PQ}}{r_{PQ}^3}, \quad (4)$$

where ϕ is a scalar potential for the resultant potential-flow field, $M(Q)$ the strength of the source, r_{PQ} the distance between a field point P and a source/vortex point Q on S or on mean lines of the lifting surface cross section, and $\Gamma_{ij}(Q)$ the strength of each U-shaped vortex filament at the i th chordwise strip (total I strips) and j th spanwise strip (total J strips). Both $M(Q)$ and $\Gamma_{ij}(Q)$ are unknowns. An integral equation is formulated to determine the strengths of the M distribution such that boundary condition (1) is satisfied. A set of linear equations with $J-1$ unknowns are set up for the strengths of the Γ_{ij} distribution such that the wake tangency conditions at K_1, K_2, \dots, K_{J-1} (Fig. 2) are satisfied.

The flow field in Ψ can therefore be computed by using Eqs. (2)-(4). The local pressure coefficient C_p , acting on the lifting surfaces, can be calculated by using the steady-state Bernoulli's equation.

$$C_p = 1 - \frac{V^2}{1/2\rho (r^2\omega^2 + V_\infty^2)} \quad (5)$$

where V is the absolute velocity from Eq. (2), V_∞ is the incoming flow velocity, and ρ is the fluid density.

INTEGRAL EQUATION FOR SOURCE-STRENGTH DETERMINATION

When the field point P is on S , Eq. (2) can be written in the N -direction as

$$V_N(P) = \frac{\partial \phi}{\partial N_P} = 2\pi M(P) - \int_S M(Q) K(P,Q) dS_Q + V_{\Gamma N}(P) \quad (6)$$

where

$$K(P,Q) = \frac{\partial}{\partial N_P} \frac{1}{r_{PQ}} \quad (7)$$

is the kernel of Eq. (6). The first term on the right-hand side of Eq. (6) stems from a local contribution of the source singularity. The term $V_N(P)$ on the left-hand side of the equation is determined by the boundary conditions (1). Equation (6) is a Fredholm integral equation of the second kind for the unknown M .

The kernel $K(P,Q)$ is singular at $Q=P$, and is asymptotically given by $K(P,Q) \approx \kappa(P)/(2r_{PQ})$, where $\kappa(P)$ is the curvature of S in the plane of \bar{r}_{PQ} and \bar{N}_P . As shown by Landweber and Macagno [12], the singularity can be removed in the following manner. Let the transpose of the kernel $K(P,Q)$ be denoted by

$$K(Q,P) = \frac{\partial}{\partial N_Q} \frac{1}{r_{PQ}} .$$

The integral

$$\begin{aligned} \int_{S+S_0} K(Q,P) dS_Q &= \int_{S_C+S_I} K(Q,P) dS_Q + \int_{S_0} K(Q,P) dS_Q + \int_{S_R} K(Q,P) dS_Q \\ &= \alpha_{C,I}(P) + \alpha_0(P) + \alpha_R(P) \end{aligned} \quad (8)$$

represents the total flux due to a "sink" of unit strength at P (referring to Eq. (3)) on S entering the region V through the remainder of $S+S_0$. When P is on S_C+S_I , then $\alpha_{C,I} + \alpha_0 = 2\pi$ and $\alpha_R = 0$; when P is on S_R , then $\alpha_{C,I} + \alpha_0 = 4\pi$ and $\alpha_R = -2\pi$. When P is on S_C+S_I or on S_R ,

$$\int_{S+S_0} K(Q,P) dS_Q = 2\pi . \quad (9)$$

With the aid of Eq. (9), Eq. (6) can be cast in the form

$$4\pi M(P) = f(P) + \int_S [M(Q) K(P,Q) - M(P) K(Q,P)] dS_Q \quad (10a)$$

for the unbounded flow case and

$$2\pi M(P) = f(P) + \int_S [M(Q) K(P,Q) - M(P) K(Q,P)] dS_Q + [2\pi - \alpha_0(P)] M(P) \quad (10b)$$

for the bounded flow case, where $\alpha_0(P)$ is the solid angle of S_0 with respect to P , as defined in Eq. (8), and $f(P) = V_N(P) - V_{\Gamma N}(P)$. Landweber [12] has shown that the limit of the mean value of the integrand in Eq. (10) is zero when Q approaches P . Thus the values of $K(Q,Q)$ need not be computed.

VORTEX FIELD AND ITS DISTRIBUTION

The flow field generated by a vortex line can be evaluated by the Biot-Savart law as shown in Eq. (4). For numerical evaluation, the vortex line is discretized into a number of straight line segments along its centerline, and each segment is represented by a vortex filament. Consider one of the filaments AB as shown in Fig. 3. The velocity field at a field point P induced by this filament is given by the Biot-Savart law,

$$\bar{v}_{AB} = \int_A^B \frac{\Gamma_{AB}}{4\pi} \frac{d\bar{h} \times \bar{r}}{r^3} \quad (11)$$

where Γ_{AB} is the constant strength of the vortex segment AB , and $d\bar{h} = \overline{AB}$.

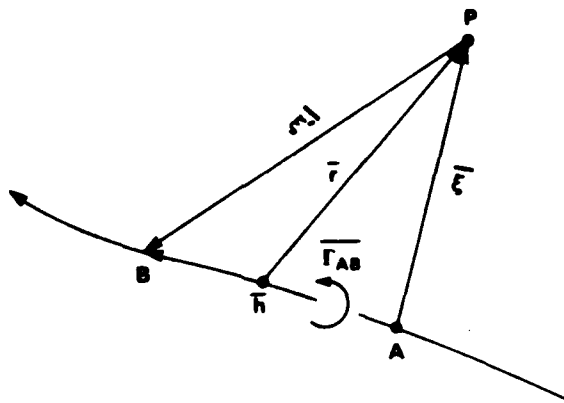


Fig. 3. Definition sketch for a vortex filament.

Denoting \overline{AP} by $\bar{\xi}$, \overline{PB} by $\bar{\xi}'$, and performing the integration in Eq. (11) yield

$$\bar{V}_{AB} = \frac{\Gamma_{AB}}{4\pi} g(\bar{h}\bar{x}\bar{\xi}) \quad (12)$$

where

$$g = \frac{1}{h^2 \xi'^2 - (\bar{h} \cdot \bar{\xi})^2} \left(\frac{h^2 - \bar{h} \cdot \bar{\xi}}{\xi'} + \frac{\bar{h} \cdot \bar{\xi}}{\xi} \right). \quad (13)$$

When P is on the segment AB or on its extension, i.e., either $\xi = 0$, or $\xi' = 0$ or $h^2 \xi'^2 - (\bar{h} \cdot \bar{\xi})^2 = 0$, the current filament AB has no contribution, i.e., $\bar{V}_{AB} = 0$. Hence, Eq. (11) is regular for the entire domain.

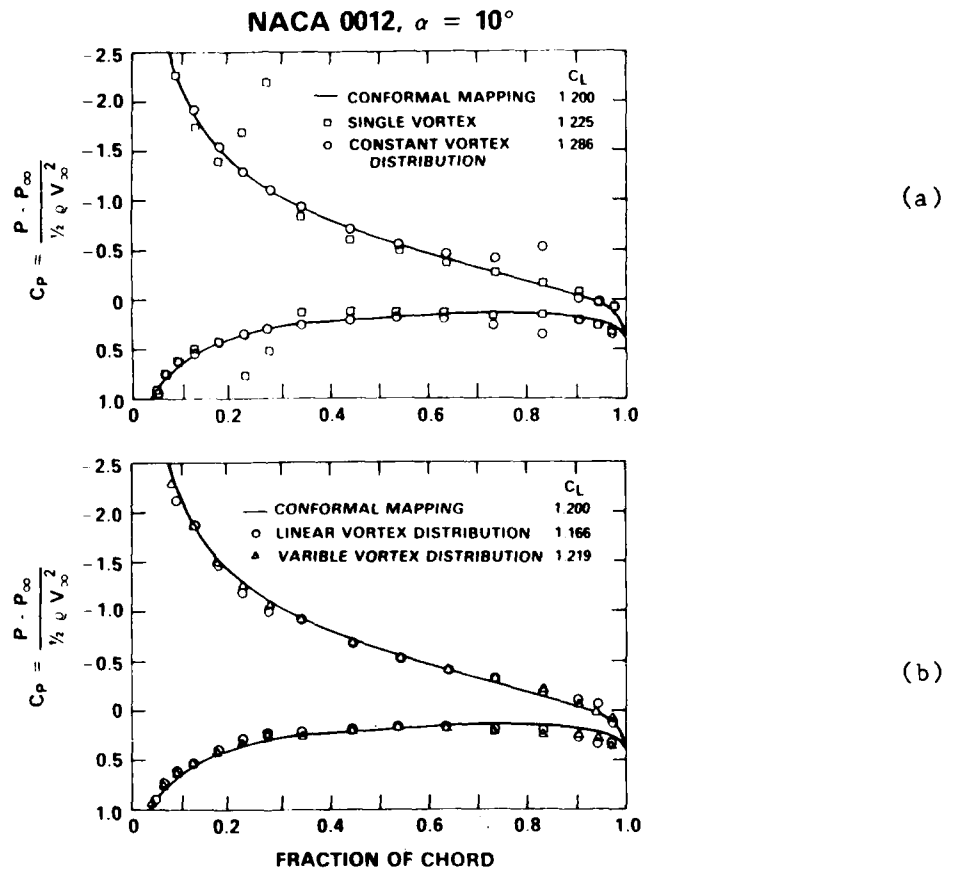


Fig. 4. Calculated pressure distributions for NACA 0012 foil at $\alpha = 10^\circ$.

In order to satisfy the wake tangency condition at the trailing edge of the blade surface, vortex filaments shown in Fig. 2 are distributed in the blade sections

tions as well as in the wake. Various distributions can be used to achieve this goal. For a thin blade representation, as commonly used in turbomachinery blade design, a mean-line distribution is used.

Numerical experiments were performed for various plausible distributions to obtain an optimized mean-line distribution. Two 2-D NACA foils, i.e., NACA 0012 and 66-209, were selected for examination. The NACA 0012 foil has zero camber and was analyzed at an angle of attack $\alpha = 10^\circ$. The NACA 66209 foil has relatively large camber and is analyzed at $\alpha = 2^\circ$. Figures 4 and 5 show four different computed pressure distributions without trailing vortices and the "exact" inviscid pressure distribution obtained by the conformal mapping procedure [13]. The first vortex distribution is the simplest selection, i.e., a single vortex at one-quarter of the

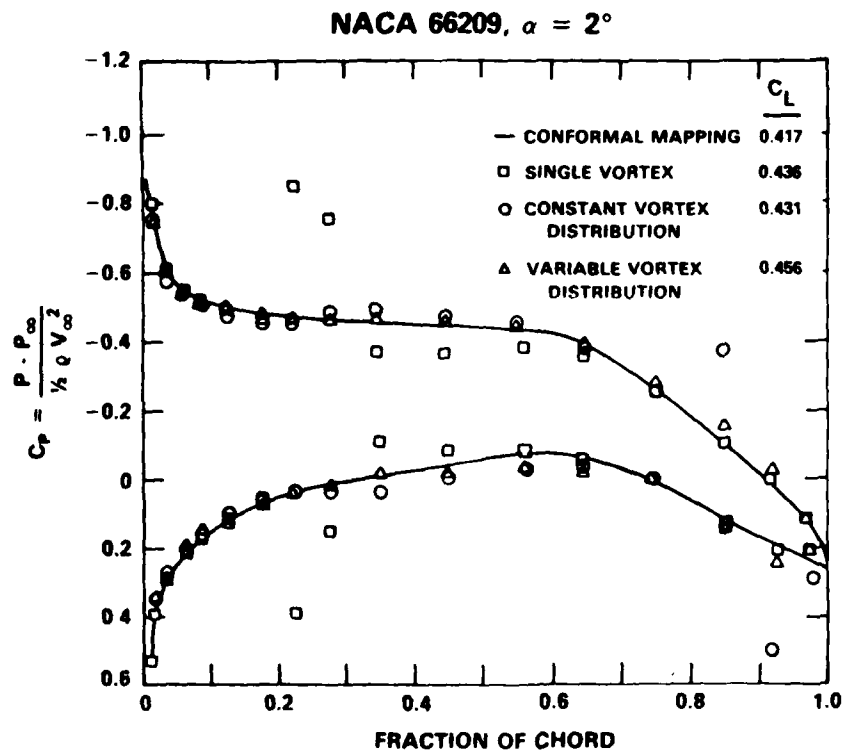


Fig. 5. Calculated pressure distributions for NACA 66-209 foil at $\alpha = 2^\circ$.

chord based on James' [14] recommendation. Surprisingly, the prediction is reasonable, except near the vortex location. The second distribution is a constant strength profile distributed chordwise between 10 and 85% of the chord. Because of the sudden drop to zero in vortex strength, a peak in C_p is predicted at $x/c = 0.85$. In order to eliminate this peak in C_p associated with the constant distribution, a linear distribution, with unit strength at $x/c = 0.10$ and zero at $x/c = 0.85$, was examined for the third distribution (omitted in Fig. 5 for clarity). Figure 4b shows not only a smooth distribution, but also a distribution conforming with the "exact" distribution. The last distribution in which the vortex strength is proportional to the local foil thickness, shown in Figs. 4 and 5, gives the best agreement with the exact solution. This distribution is used for the extension to the 3-D case.

The vortex distribution for the 3-D lifting surface as shown in Fig. 2 consists of bound vortices and trailing vortices. A bound vortex segment at the i th chordwise strip and j th spanwise strip is a portion of a U-shaped vortex filament, of strength Γ_{ij} , which propagates downstream to infinity. The wake tangency condition is satisfied at the Kutta point K_j . The vortex strength of the segment ij is

$$\Gamma_{ij}(x_i, s_j) = T(x_i, s_j) \gamma(s_j) h(x_i) \quad \begin{array}{l} i = 1, \dots, I-1 \\ j = 1, \dots, J-1 \end{array} \quad (14)$$

where T is the blade thickness distribution, γ is the bound vortex strength in the spanwise (s_j) direction, and h is defined as the piecewise length of the vortex filament along the chord. The $J-1$ algebraic equations are formulated for $\gamma(s_j)$.

For lifting surfaces without rotation, the trailing vortex filaments are parallel to the incoming flow. For surfaces with rotation, the trailing vortex filaments are defined by

$$x = r_t \sin\theta, \quad y = r_t \cos\theta, \quad z = z_t + V_\infty\theta/\omega \quad (15)$$

where the subscript t refers to the trailing edge, and θ is the azimuthal angle measured from the trailing edge.

NUMERICAL ITERATION

The two integral Eqs. (10a) or (10b) for the source strengths and the algebraic equations for the vortex strengths are coupled and should be solved simultaneously. In the present approach, a global iterative procedure is used to obtain solutions for both singularity strengths. In order to eliminate a large matrix inversion, the integral Eq. (10) for M is solved iteratively also. Only the small set of algebraic equations for Γ is solved by Gaussian elimination procedure. The Neumann iteration formula is used in this approach to solve Fredholm integral equations of the second kind. Hence, Eqs. (10a) and (10b) can be cast in the form

$$4\pi M^{(n+1)}(P) = f^{(n)}(P) + \int_S [M^{(n)}(Q)K(P,Q) - M^{(n)}(P)K(Q,P)] dS_Q \quad (16a)$$

for the unbounded flow case and

$$2\pi M^{(n+1)}(P) = f^{(n)}(P) + \int_S [M^{(n)}(Q)K(P,Q) - M^{(n)}(P)K(Q,P)] dS_Q \\ + [2\pi - \alpha_0(P)]M^{(n)}(P) \quad (16b)$$

for the bounded flow case, where n is the number of the iterations and $f^{(n)}(P) = V_N(P) - V_{\Gamma N}^{(n)}(P)$. Although the iteration between sources and vortices is decoupled in the global iteration, the interaction between them is included through the variation of $f(p)$ between iterations.

One must select a first approximation in order to start the iterations. In applying the Neumann iteration formula, the usual choice is $M^{(1)}(P) = V_N(P)/2\pi$ for Eq. (6). However, as was shown in [12] for the unbounded-flow case, this choice may result in slow convergence of the iterations and a preferable first approximation is given by [12] as $M^{(1)}(P) = V_N(P)/4\pi$. The same value was also selected for the bounded-flow case.

NUMERICAL EXAMPLES

Two sets of numerical results are presented to illustrate the foregoing proce-

dure. The first is for an unbounded flow case; namely a marine propeller tested in open water [15,16]. The second is for a bounded flow case; namely an axial-flow pump.

GEOMETRY INPUTS

The surface S depicted in Fig. 1, on which the sources are to be distributed, is divided into small panels, each with constant source strength. On each panel a representative point is chosen, where the boundary condition, Eq. (1), will be enforced. The panel area acts as a weighting factor in the calculation, and the surface normal at the representative point defines the panel orientation. The axisymmetric boundary surface is divided into sectors corresponding to the number of blades of the rotor. Surface-panel generation is conducted in detail for only one of these sectors. Panels for the remaining sectors are then generated simply by rotating the basic set. Figures 6 and 7 show a total of 1,650 panels for a 3-blade marine propeller in open water and a total of 3,870 panels for a 5-blade axial-flow pump. The marine propeller is DTNSRDC controllable-pitch Propeller 4718, with the diameter

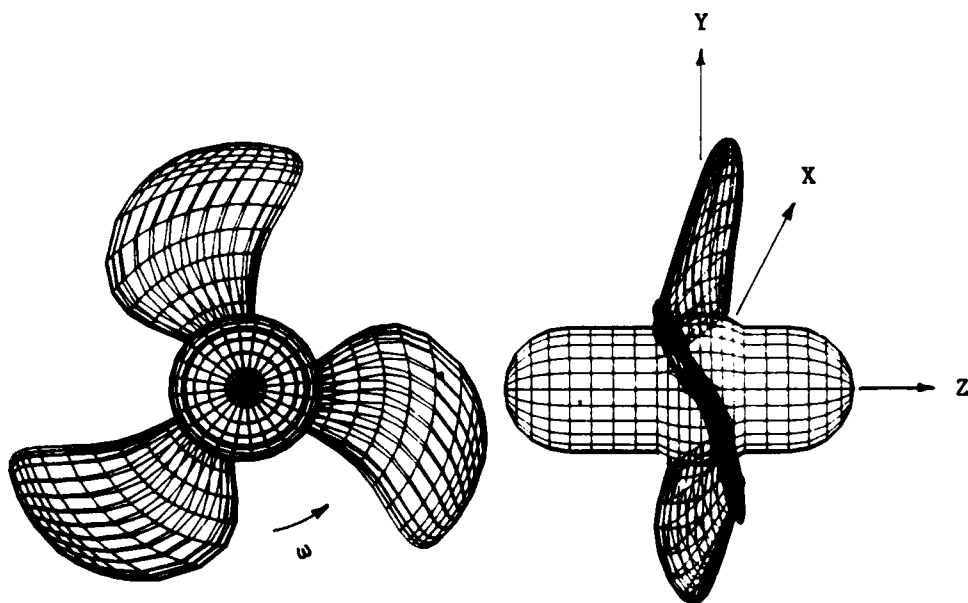


Fig. 6. Paneling on the marine propeller.

$D = 0.61$ m, an Expanded-Area-Ratio (EAR) of 0.44 and a tip skew of 20° .

The upstream supporting strut used in the measurements is terminated about one propeller radius upstream of the propeller plane in the calculation model. The axial-flow pump has a casing diameter $D = 1.04$ m. The hub diameter varies from $0.35D$ to $0.66D$ in the blade section.

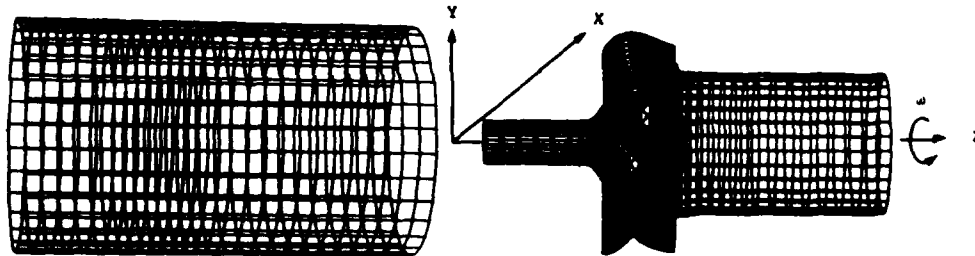


Fig. 7. Paneling on the axial-flow pump.

NUMERICAL RESULTS

The steady pressure distribution was calculated on the surface of Propeller 4718 at the design advance coefficient, $J = 2\pi V_\infty / \omega D = 0.751$. Figure 8 shows the generated

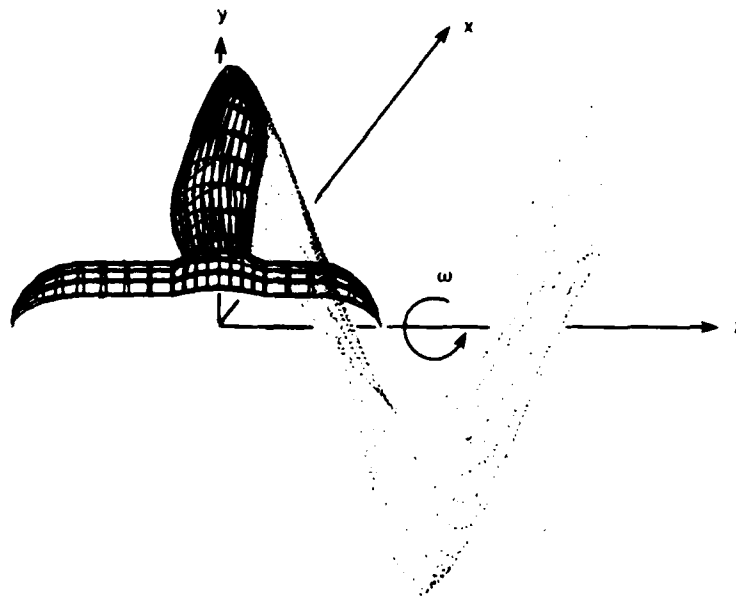


Fig. 8. Wake vortex filaments and grids of one sector for Propeller 4718 at $J = 0.751$.

wake vortex pattern under the operating condition by using Eq. (15). The wake terminates at about 1.5 propeller radii from the trailing edge. The computational results show that the flow around the blade is not affected by even doubling the wake vortex filament length. Convergence of the solution was obtained after 15 iterations. In Fig. 9, the predicted pressure coefficients normalized with respect to local dynamic pressure as defined in Eq. (5) are compared with experimental measurements [15,16] on the blade surface at four different radii, i.e. $2r/D = 0.5, 0.7, 0.8$ and 0.9 , with the propeller operating in uniform flow. The measurements at $2r/D = 0.8$ were only taken on the suction side. Three pressure distributions are shown at each radius of Fig. 9: (1) measured pressure distribution, (2) distribution calculated by Kim and Kobayashi [17] using a vortex-lattice method (labeled as PSF2), and (3) distribution calculated by the present method (labeled as IPF3D). The calculated results using the present approach, i.e., IPF3D, agree very well with the measured data except near the trailing edge for $2r/D = 0.5$ and 0.7 . This discrepancy near the trailing edge is due to the wake tangency condition used at the trailing-edge Kutta point, which depends strongly on the direction given in input data. Predictions of PSF2 are lower than the measured as well as the current calculated pressures. In their paper, Kim and Kobayashi also presented calculated and measured data for the propeller at two different values of the advance ratio J . The calculated and experimental results compare more favorably in the case of a NSMB propeller than in the case of Propeller 4718. This is thought to be due to the following reasons: (i) the NSMB propeller is more heavily loaded than Propeller 4718. (The vortex lattice method [5,6] usually predicts more accurately for a highly cambered lifting surface) and (ii) Propeller 4718 has a tip skew angle of 20° as compared to 0° for the NSMB propeller. (PSF2 uses induced velocities from other thickness-dominated components at the propeller plane as inputs to represent the complete

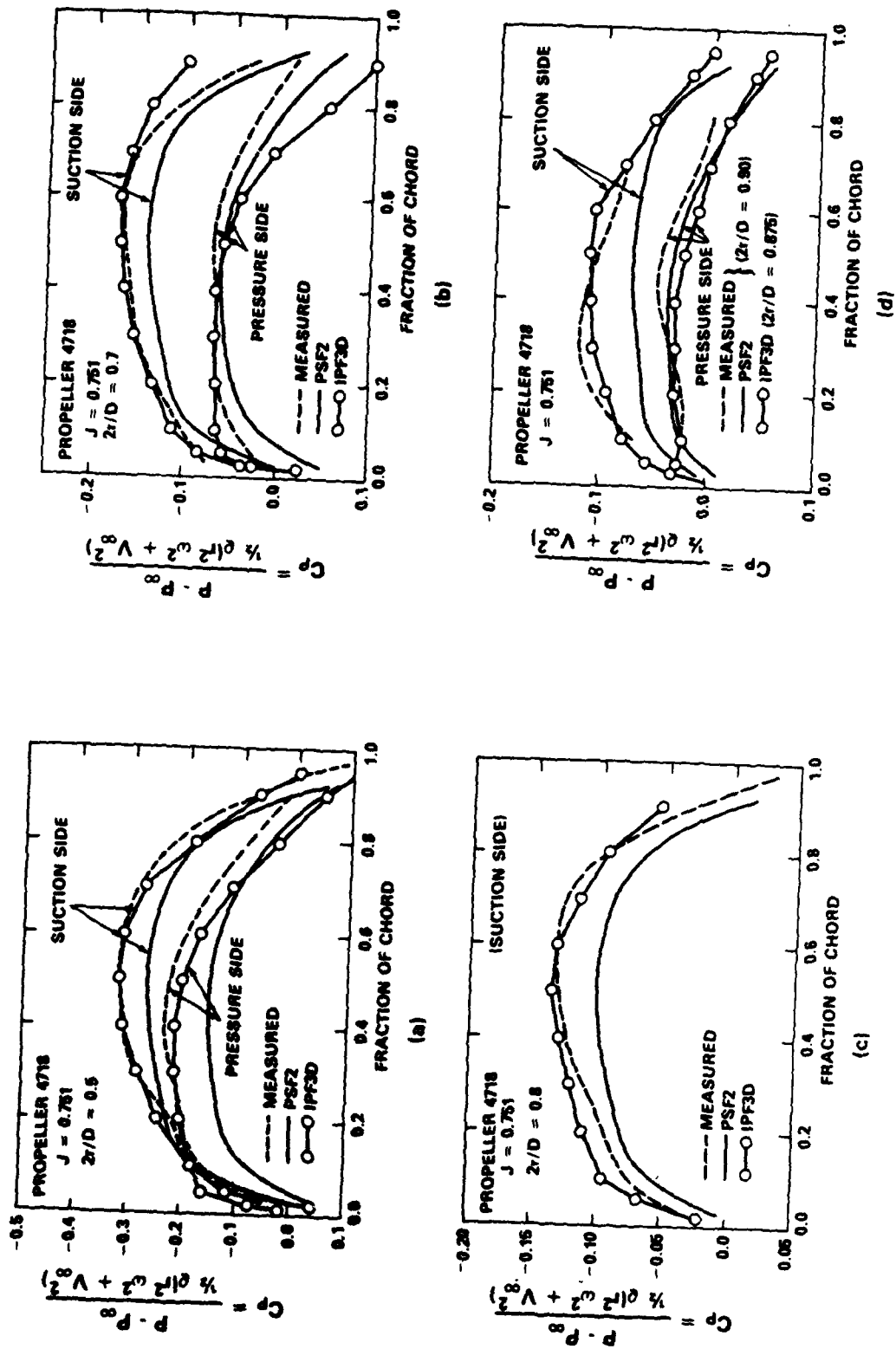


Fig. 9. Pressure distributions on Propeller 4718 at $J = 0.751$.

blade surface boundary conditions. The deviation becomes large when the skew angle is large.) These two difficulties apparently do not occur in the method presented in this paper.

Figure 10 shows the suction-side pressure distributions at two radii, i.e. $2r/D = 0.5$ and 0.8 , for three off-design conditions. Because the measurements were only performed on the suction side, the calculated distribution on the pressure side is not included. Based on the computed results on the NSMB propeller and a 2-D conformal-mapping calculation, Hess [7] concludes that the leading-edge pressure

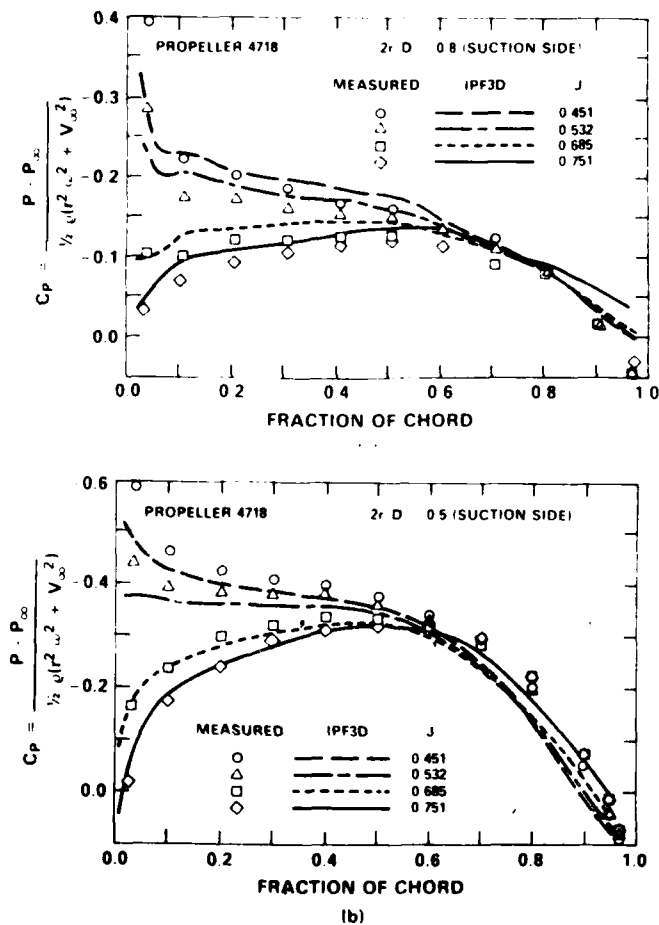


Fig. 10. Pressure distributions on Propeller 4718 at different values of J .

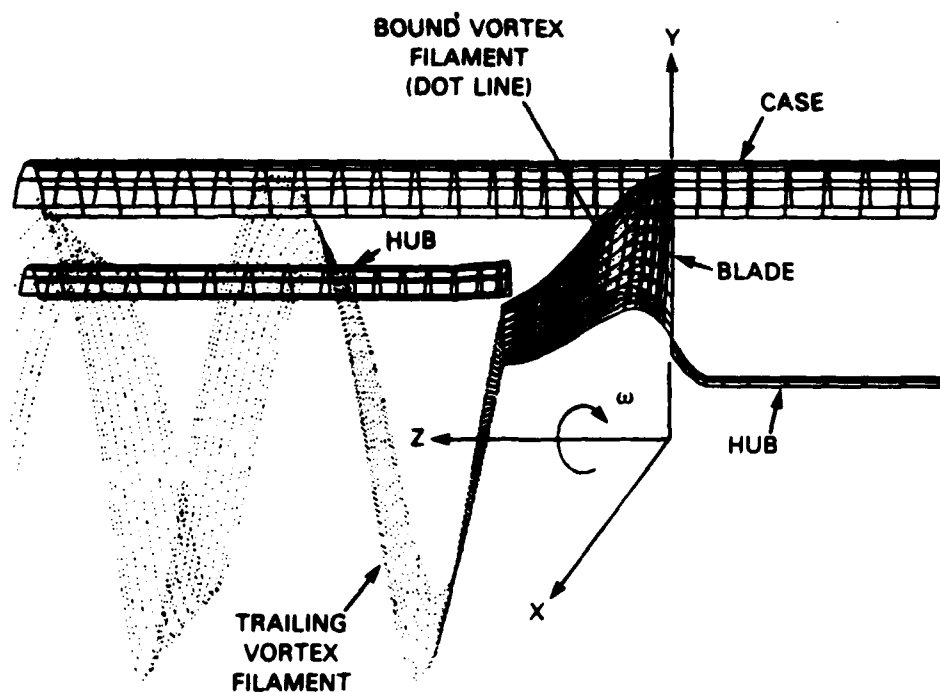


Fig. 11. Wake vortex filaments and grids of one sector for axial-flow pump at $c = 0.292$.

peak exists on the pressure side for off-design condition. However, results from the present calculation for Propeller 4718 do not show this peak, which may be due to the stronger three-dimensional relief for the higher skew blade of Propeller 4718.

The axial-flow pump used as a calculation example is a lightly loaded machine equipped with sharp leading- and trailing-edge blades. Measurement data are not available for comparison. The calculated results are shown here to demonstrate the feasibility of the methodology for an internal flow with an axially rotating impeller. The flow coefficient c , defined as the ratio of V_{∞} to the blade tip speed is 0.292. Figure 11 shows the wake pattern of the vortex filaments, generated by Eq. (14), associated with $c = 0.292$. The vortex filaments extend $1.83D$ downstream from the blade trailing edge. The boundary condition for the inlet panels is 4m/sec . Figure 12

shows the computed pressure distributions on both suction and pressure sides of the blade for two strips parallel to the hub. The comparisons are made for two different grids used in the calculations. The fine grid has (1580 panels in each blade sector) twice the number of panels as compared to the coarse grid (774 panels). The predicted pressure distributions, shown in Fig. 12, for both grids are obtained after 19 global iterations. The agreement of these results indicates the adequacy of the coarse grid calculation. Figure 12 also shows the panel distribution on the blade for the coarse grid. Figure 13 shows transverse velocity distributions, i.e. the vector sum of the tangential and the radial components of the computed velocity

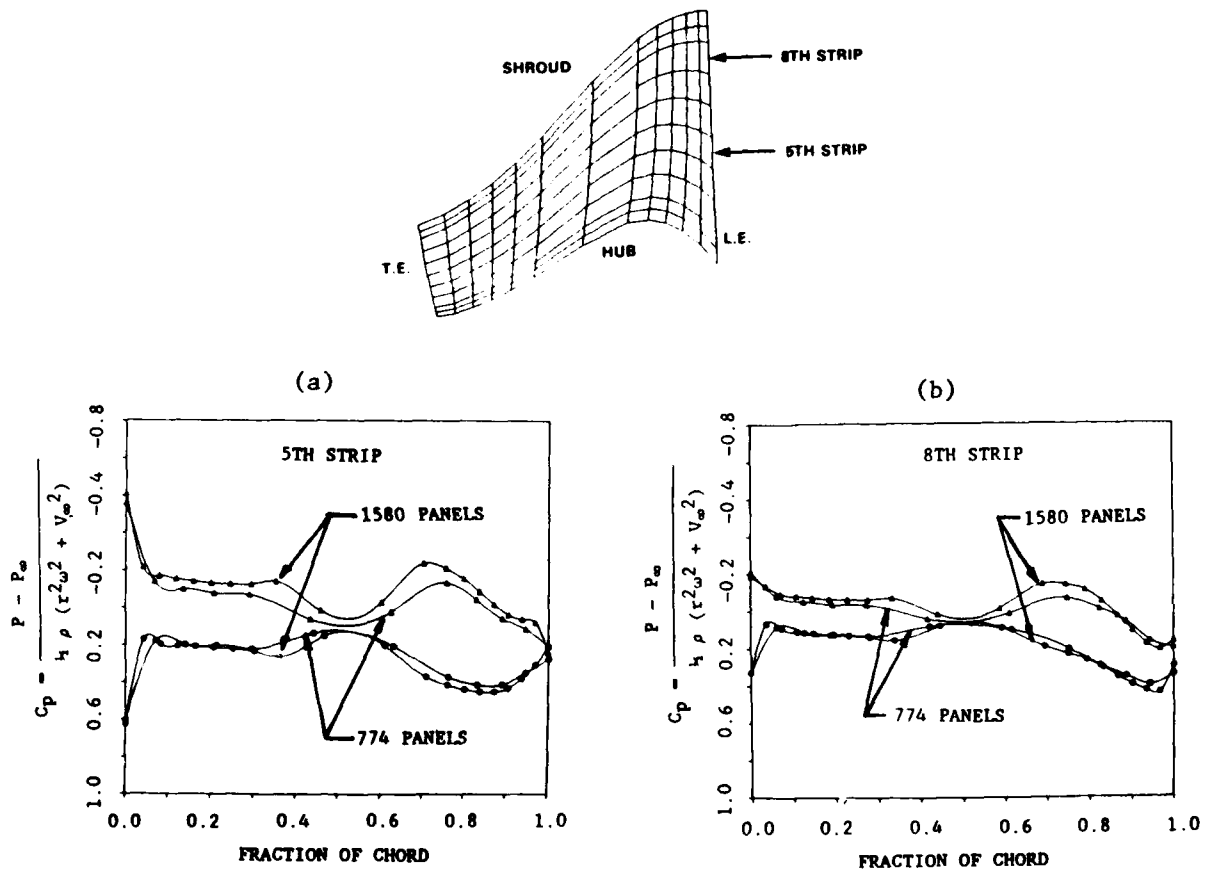


Fig. 12. Calculated blade pressure distributions for axial-flow pump at $c = 0.292$ for (a) 5th strip, (b) 8th strip.

at two sections of $0.11D$ and $0.6D$ downstream of the trailing edge. Due to the prescribed wake vortex filaments and the proximity of the velocity computing point to the vortex centerline and hub or shroud surfaces, a few unrealistically large velocity vectors are seen in Fig. 13. The mass flowrates across these sections are within 3-6% of the inlet condition. The calculated energy transfer rate, defined as the difference in angular momentum between an inlet and an outlet, is within 8% of the design value.

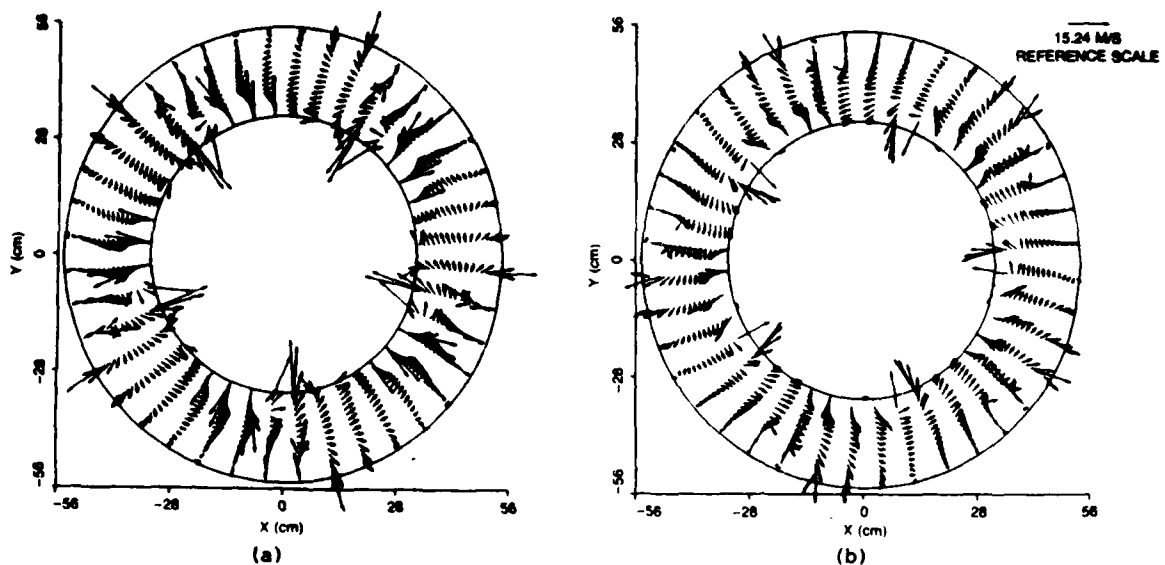


Fig. 13. Computed transverse-velocity distribution at (a) $z = 0.11D$, (b) $z = 0.60D$ from the trailing edge for axial-flow pump.

CONCLUSIONS

1. An integral-equation/singularity-method approach to the problem of computing flow past a rotating element with lift-generating surfaces is feasible when using source distributions for both solid boundaries and a permeable inlet flow control boundary, and bound vortex and wake trailing vortex filaments for lifting surfaces.

2. With a slight variation in the governing integral equation, the method can be applied to both internal and external rotating axial flows.
3. An effective mean-line vortex strength distribution, described by Eq. (14), has been obtained for the representation of the lifting surfaces.
4. The Neumann iteration scheme, as compared to the matrix inversion scheme, has been shown to be efficient and accurate.
5. The global iteration between the source strengths in the integral equations and the vortex strengths in the algebraic equations converges fairly rapidly. This iterative procedure was used in conjunction with the Neumann iteration scheme and found to accelerate the convergence for both iteration processes.

REFERENCES

1. Miranda, L.R., "Application of Computational Aerodynamics to Airplane Design," *Journal Aircraft*, Vol. 21, No. 6, pp. 355-370 (1984).
2. Margason, R.J., S.O. Kjelgaard, W.L. Sellers and C.E.K. Morris, "Subsonic Panel Methods - A Comparison of Several Production Codes," AIAA 23rd Aerospace Meeting, Paper No 85-0280, Reno, Nevada (1985).
3. Desy, N., H. Do and N. Nuon, "Turbine Casing and Distributor Hydraulic Design," WATERPOWER '87, Session No. 13, Portland, Oregon (1987).
4. Greeley, D.S. and J.E. Kerwin, "Numerical Methods for Propeller Design and Analysis in Steady Flow," SNAME Transactions, Vol. 90, pp. 415-453 (1982).
5. Coney, W.B., C.Y. Hsiu and J.E. Kerwin, "A Vortex Lattice Lifting Line Program for Single and Multi-Component Propulsors," MIT-PLL-2, Report and User's Manual (1986).
6. Kerwin, J.E., S.A. Kinnas, J.T. Lee and W.Z. Shih, "A Surface Panel Method for the Hydrodynamic Analysis of Ducted Propellers," presented at SNAME Annual Meeting, New York (1987).
7. Hess, J.L. and W.O. Valarezo, "Calculation of Steady Flow About Propellers Using a Surface Panel Method," *Journal of Propulsion*, Vol. 1, No. 6, pp. 470-476 (1985).
8. Hess, J.L., "Calculation of Potential Flow About Arbitrary Three-Dimensional Lifting Bodies," McDonnell Douglas Report No. MDC J5679-01 (1972).
9. Maskew, B., "A Computer Program for Calculating the Non-Linear Aerodynamic Characteristics of Arbitrary Configurations," Analytical Methods, Inc., Report (1983).
10. Morino, L., "A General Theory of Unsteady Compressible Potential Aerodynamics," NASA CR 2464 (1974).

REFERENCES (Continued)

11. Nathman, J.K. and J.H. Frank, "Application of VSAERO to Internal Flows," AIAA 5th Applied Hydrodynamic Conference, Paper No. 87-2415, Monterey, California (1987).
12. Landweber, L. and M. Macagno, "Irrotational Flow About Ship Forms," The University of Iowa, IIHR Report No. 123 (1969).
13. Halsey, N.D., "Potential Flow Analysis of Multi-Element Airfoils Using Conformal Mapping," AIAA Journal, Vol. 17, pp. 1281-1288 (1979).
14. James, R.M., "On the Remarkable Accuracy of the Vortex Lattice Method," Computer Methods in Applied Mechanics and Engineering, Vol. 1, No. 1, pp. 59-79 (1972).
15. Jessup, S.D., "Measurement of the Pressure Distribution on Two Model Propellers," DTNSRDC Report 82/035 (1982).
16. Jessup, S.D., "Further Measurements of Model Propeller Pressure Distributions Using a Novel Technique," DTNSRDC Report 86/011 (1986).
17. Kim, K.H. and S. Kobayashi, "Pressure Distribution on Propeller Blade Using Numerical Lifting-Surface Theory," Proceedings of the SNAME Symposium - Propellers '84, Virginia Beach, Virginia (1984).

INITIAL DISTRIBUTION

Copies	Copies
1 DARPA/Wisniewski	7 NAVSEA
3 ONR	1 SEA 05R32 (A. Smookler)
1 1132F (Reichman)	1 SEA 55W3 (E. Comstock)
1 1132F (Whitehead)	1 SEA 55W31 (G. Jones)
1 1245 (Hansen)	1 SEA 55X33 (W. Sandberg)
1 ONR/Boston	1 SEA 56X7 (C. Crockett)
1 ONR/Chicago	1 SEA 56Y11 (F. Saavedra)
1 ONR/New York	1 SEA 56Y13 (R. Wagner)
1 ONR/Pasadena	1 NAVFAC/032
1 ONR/San Francisco	1 NADC
2 NRL	12 DTIC
1 Code 2027	1 AFOSR/NAM
1 Code 2629	2 MARAD
3 USNA	1 Division of Ship R&D
1 Tech Library	1 Library
1 Naval Systems Engr. Dept.	1 NASA/HQ/Library
1 B. Johnson	2 NASA/Ames Research Center
1 NAVPGSCOL/Library	1 D. Kwak
1 NOCS/Library	1 Library
1 NCSC/712	2 NASA/Langley Research Center
1 NCEL/131	1 Library
1 NSWC, White Oak/Library	1 D. Bushnell
1 NSWC, White Oak/Library	1 NBS/Library
1 NUSC/Library	1 LC/Science & Technology
1 ONT	3 U of Cal, Berkeley/Dept Naval Arch
1 211 (J. Gagorik)	1 Library
2 CIT	1 W. Webster
1 Aero Library	1 R. Yeung
1 A.J. Acosta	1 Calif State U, Long Beach
	1 Cebeci
	1 Catholic U of Amer/Civil & Mech Engr
	1 U of Virginia/ Aero Eng. Dept

INITIAL DISTRIBUTION

Copies

4 Univ of Iowa
 1 Library
 1 V.C Patel
 1 L. Landweber
 1 F. Stern

5 MIT
 1 Library
 1 J.R. Kerwin
 1 T.F. Olgilvie
 1 J.N. Newman
 1 P. Leehey

2 Univ of Michigan/NAME
 1 Library
 1 T. Brockett

3 Penn State
 1 C.L. Merkle
 1 R.E Henderson
 1 ARL Library

1 Gibbs & Cox/Tech Info

1 Gould Defense System, Inc.
 1 Meng

1 Grumman Aerospace Corp/ Library

2 HRA, Inc
 1 Cox
 1 Scherer

1 Lockheed, Georgia Co/Library

2 McDonnell Dougless, Long Beach
 1 T. Cebeci
 1 J.L. Hess

1 Newport News Shipbuilding/Library

Copies

2 SIT
 1 McKee
 1 Library

1 VPI
 1 Schetz

2 Webb Institute
 1 Library
 1 Ward

1 SNAME/Tech Library

1 National Science Foundation/
 Engr Division Library

1 Boeing Company, Seattle
 1 Marine System

1 Bolt, Beranek & Newman/Library

1 General Dynamics, EB/Boatwright

1 TRW Systems Group/Library

1 United Technology/East Hartford, CT

1 Westinghouse Electric/Research
 1 E.A. Owen

1 Westinghouse Electric/Nuclear
 1 S.K. Chow

1 Propulsion Dynamics, Inc

1 Propulsion System, Inc

1 Sun Shipbuilding/Library

1 Northrop Corp/Aircraft Division

1 Nielsen Engr & Research

CENTER DISTRIBUTION

Copies	Code	Name	Copies	Code	Name
1	0120		1	1561	Cox
1	12		1	1562	Davis
1	012.1	Nakonechny	1	1563	Milne
1	012.4	Cathers	1	1563	Moran
1	15	Morgan	1	1564	Feldman
1	1506	Hawkins	1	1802	Lugt
1	1508	Boswell	1	1843	Hausling
6	1509	(microfiche)	1	19	Sevik
1	152	Lin	1	1905	Blake
1	1521	Day	1	27	Arigo
1	1522	Wilson	1	2704	Quandt
1	1522	Remmers	1	272	Doyle
1	154	McCarthy	1	272	Huang
1	1542	Huang	1	272	Nickerson
20	1542	Lee	1	2720	Urbach
10	1542	Jiang	1	2721	Stricker
1	1543	Purtell	1	2721	Purnell
1	1544	Peterson	10	2722	Bein
1	1544	Dai	1	274	Wang
1	1544	Hubbard	1	2741	Henry
1	1544	Jessup	1	2741	Calvert
1	1544	Kim	10	5211.1	Reports Control
1	1544	Schott	1	522.1	TIC (C)
1	1544	Yang	1	522.2	TIC (A)
1	156	Cieslowski			

ATE
LMED
8